

Geometric Time-Domain Identification of Three-Phase Load Equivalents from Terminal Measurements

Francisco G. Montoya, Francisco de Leon, *Fellow, IEEE*, Francisco M. Arrabal-Campos, and Alfredo Alcayde

Abstract—This paper presents a geometric time-domain method for identifying three-phase load equivalents from instantaneous voltage and current measurements at the point of common coupling. Measured waveforms are interpreted as trajectories in Euclidean signal spaces, and load-equivalent parameters are recovered from the geometry of those trajectories. The method extends a previously published single-phase geometric identification formulation to three- and four-wire systems and places special emphasis on the three-wire case, where no neutral voltage is measured and the terminal data must satisfy coupled Kirchhoff constraints. The main advance over the earlier analytical formulation is a sampled-data implementation based on local time windows, normalized matrix equations, harmonic-projection derivative and primitive coordinates, explicit geometric identifiability tests, passivity constraints, and energy/Kirchhoff residuals. The method does not force a model when the measured trajectory lacks enough information; instead, it reports low-rank or ill-conditioned windows as low-confidence evidence. Numerical simulations with clean data, measurement noise, window-length sweeps, and sensor delay show that the method accurately identifies informative three-phase trajectories and exposes structurally degenerate cases such as pure single-frequency excitation for higher-order three-wire models. For a given admissible topology the identified circuit closes the instantaneous terminal energy balance of the measured load over the analysis window.

Index Terms—Euclidean waveform geometry, geometric algebra, Load-equivalent parameter identification, load modeling, power systems, three-phase loads, time-domain methods, unbalanced systems.

I. INTRODUCTION

MODERN power systems are increasingly measured, controlled, and protected through digital platforms. In this context, equivalent load and network-section parameters are no longer only planning data; they can become real-time state information for protection, monitoring, converter control, and adaptive operation [1], [2]. Most measurement-based load-identification methods estimate aggregate static or dynamic parameters from events, disturbance records, phasor-domain quantities, or optimization models [3]–[5]. Those approaches are essential for system-level studies, but they are not designed to recover an element-level energetic equivalent directly from the instantaneous terminal waveforms of a measured load or feeder section.

A different school of thinking starts from the time-domain geometry of the measured waveforms. Geometric algebra provides a compact language for subspaces, oriented hypervolumes, and differential-geometric constructions [6], [7]. In power-system waveform applications, this view is closely related to identifying

physical load-equivalent elements from trajectory geometry rather than from a phasor fit or a spectral power decomposition [8]. The single-phase geometric identification method published in 2021 formalized this idea by constructing a waveform space vector we coined *spacor*, whose osculating subspace yields closed-form expressions for R , L , and C parameters [9]. That earlier study was mainly theoretical and analytical: it proved that the parameters can be computed from terminal time-domain data when the required geometric information is present.

Subsequent experimental validation showed that the single-phase method can be operated with laboratory measurements, provided that numerical differentiation, acquisition noise, and finite records are treated methodologically [10]. The present paper takes the next step. It extends the identification problem to three-phase equivalents, with special attention to three-wire systems where no neutral potential is available. It also introduces the sampled-data layer needed to make the theory operational in this setting: finite windows, matrix equations, window-local derivative and integral coordinates, normalization, and diagnostic screening.

The three-phase extension is not a simple repetition of three independent single-phase identifications. In four-wire systems, phase-to-neutral voltages make a phase-wise formulation possible. In three-wire systems, however, branch variables are hidden behind line-to-line voltages and constrained line currents. Delta parallel and wye series equivalents may also become difficult to distinguish if the local waveform trajectory has insufficient rank. A practical method must therefore identify parameters and, at the same time, quantify whether the measured window contains enough information to support the chosen physical equivalent.

This paper concentrates on the identification problem. It does not attempt to introduce a complete power theory; instead, it uses energy conservation as an internal physical validation criterion for the identified equivalent. The identification itself is not accepted only because a set of parameters fits the terminal equations. A candidate equivalent must also close the instantaneous energy balance implied by its resistors, inductors, and capacitors. This energy-admissibility criterion is a new practical layer of the method and is used here as a physical validation gate for every processed window.

The manuscript develops a unified formulation for three-phase wye and delta equivalents in three- and four-wire systems, and then turns the published geometric construction into a windowed matrix estimator that can be applied directly to sampled terminal records. The implementation adds a derivative and primitive reconstruction layer based on harmonic projection, FIR filters, polynomial fits, or regularized finite differences, avoiding high-order pointwise differentiation. It

F. G. Montoya, F. M. Arrabal-Campos, and A. Alcayde are with the Department of Engineering, University of Almeria, Spain. F. de Leon is with the Department of Electrical and Computer Engineering, New York University, USA.

also makes identifiability explicit through the geometric rank and conditioning of the local time-domain trajectory. It adds the energy-admissibility test so that a numerically fitted equivalent is accepted only when it closes the terminal energy balance. Because each window reduces to a fixed-topology least-squares problem, the computational cost remains small and explicit. The numerical evidence is then built from analytically controlled cases and realistic MATLAB simulations with unbalanced multisine feeders, measurement noise, gain and offset errors, quantization, moving-average acquisition effects, window-length sweeps, coherent current-sensor delay, and low-information cases that must be screened out rather than over-fitted.

Taken together, these tests give a consistent quantitative picture. In the controlled three-wire delta and wye cases the windowed estimator reproduces the analytical branch constants and closes the terminal power balance at machine precision, with the residual rising only to the injected noise floor (of order 10^{-3}) under 60 dB measurement noise. In the realistic 20 kHz multisine simulations, practical windows of 0.5–2 cycles keep the recovered branch R , L , and C values within a 5% engineering band under clean data, 60 and 40 dB noise, 12-bit quantization, and gain mismatch. The energy-admissibility gate accepts fifteen of the twenty-one practical-window configurations and rejects exactly the six affected by a 50 μ s current-sensor delay, where the parameter error grows to about 37%. The method therefore recovers physical parameters under ordinary measurement imperfections and, just as important, flags a coherent timing bias instead of disguising it as a reliable equivalent.

The practical value of this method is that it determines an equivalent circuit which, for the assumed admissible topology, closes the terminal energy balance of the measured load over the analysis window. The energy residual is an admissibility check for the identified terminal equivalent, not a claim that terminal data uniquely determine the physical internal energy localization. The identified R , L , and C elements therefore form a physically structured equivalent rather than a black-box fit.

The specific contributions of this paper, relative to the single-phase geometric method of [9] and its experimental validation in [10], are as follows.

- A unified three-phase, three- and four-wire formulation of the geometric load equivalent, covering both wye and delta connections under coupled Kirchhoff constraints with no measured neutral voltage.
- A topology-dependent observability analysis that identifies which branch forms are directly recoverable and proves the structural singularity of the series-delta and parallel-wye three-wire cases.
- A windowed matrix estimator that realizes the geometric (osculating-subspace) construction numerically over a finite sampled window, with harmonic-projection derivative and primitive coordinates.
- An explicit identifiability layer based on the geometric rank and conditioning of the local time-domain trajectory, screening low-information windows rather than over-fitting them.
- An energy-admissibility gate that accepts an identified equivalent only when it closes the instantaneous terminal energy balance over the analysis window.

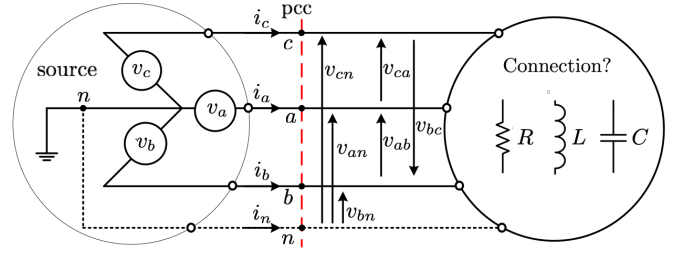


Figure 1. Three-phase load identification from terminal measurements at the PCC.

This paper addresses identification. The element-level energy accounting that the identified equivalents enable is pursued in separate work [11].

II. THREE-PHASE LOAD EQUIVALENTS AND IDENTIFICATION EQUATIONS

The problem is to identify an equivalent three-phase load from measurements of instantaneous voltages and currents at the point of common coupling (PCC), as shown in Fig. 1. The equivalent is required to reproduce the measured terminal behavior and to provide a physically interpretable set of parameters over the local observation window.

For a four-wire system, phase-to-neutral voltages are available or can be directly measured. Each phase can therefore be treated as a single-phase identification problem with a chosen branch topology. This problem was solved in [9] and experimentally validated in [10]. For a three-wire system, only line-to-line voltages are available and the line currents satisfy

$$i_a + i_b + i_c = 0, \quad v_{ab} + v_{bc} + v_{ca} = 0. \quad (1)$$

The absence of a measured neutral makes the three-wire case a complex technical problem.

The identification process is as follows. First, a candidate topology is selected: wye or delta, and series or parallel branches. Second, a space vector, or *spacor*, is built from the measured terminal variables and the derivatives or integrals required by the chosen branch law. Third, KCL and KVL are used to express the measured trajectory as a lower-dimensional object embedded in a higher-dimensional Euclidean space. Finally, the multivector associated with the model subspace is compared with the osculating multivector obtained from the measured trajectory. In the symbolic version this comparison produces closed-form quotients for R , L , or C . In the sampled-data version used here, the same equations are evaluated over finite windows and screened by rank, conditioning, passivity, and residual diagnostics.

A. Equivalent Model Families

The model library starts from the two basic three-phase connections shown in Figs. 2 and 3. Each branch can be represented by a series or parallel RLC equivalent, as in Fig. 4. Simpler submodels are obtained by suppressing terms that are not required or not identifiable in a local window.

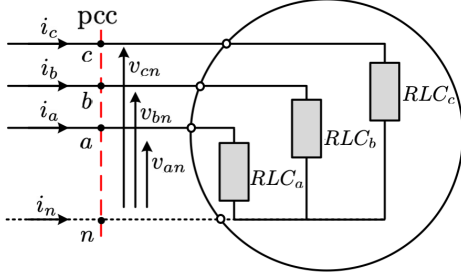


Figure 2. Wye-connected three-phase equivalent. In four-wire systems the neutral is measurable; in three-wire systems it may be virtual or absent.

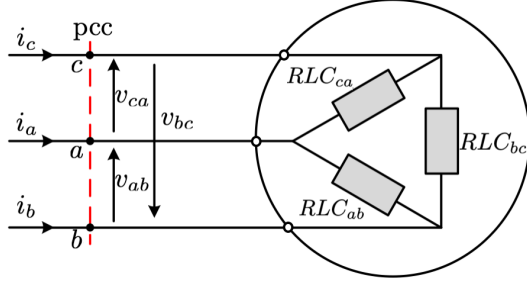


Figure 3. Delta-connected three-wire equivalent. Branch variables are inferred from line-to-line voltages and line currents.

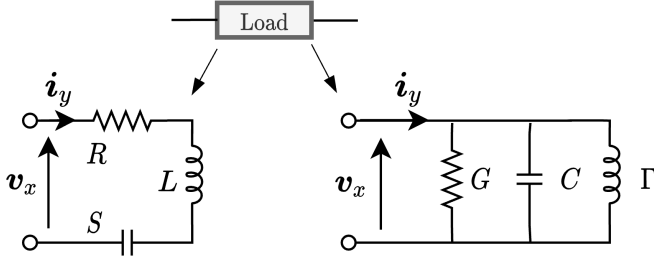


Figure 4. Series and parallel RLC branch models used to build the three-phase library.

1) *Four-Wire Wye Model*: When phase voltages v_{an} , v_{bn} , and v_{cn} are available, a parallel branch model can be written as

$$i_x(t) = G_x v_{xn}(t) + \Gamma_x \check{v}_{xn}(t) + C_x v'_{xn}(t), \quad x \in \{a, b, c\}, \quad (2)$$

where v' denotes time derivative and \check{v} time integral of v , respectively, and $\Gamma = 1/L$. A series branch model is

$$v_{xn}(t) = R_x i_x(t) + L_x i'_x(t) + S_x \check{i}_x(t), \quad S = 1/C. \quad (3)$$

These equations are the phase-wise version of the single-phase method in [9]. The four-wire case is included for completeness, while the three-wire case is the focus of this paper.

2) *Three-Wire Delta Parallel Model*: For a three-wire load, the directly resolvable delta family is the parallel branch form. The reason is physical and geometric: the branch voltages of a delta are exactly the measured line-to-line voltages, and the measured line currents are obtained from KCL differences of

the internal branch currents. For a delta parallel equivalent,

$$i_{ab} = G_{ab} v_{ab} + \Gamma_{ab} \check{v}_{ab} + C_{ab} v'_{ab}, \quad (4)$$

$$i_{bc} = G_{bc} v_{bc} + \Gamma_{bc} \check{v}_{bc} + C_{bc} v'_{bc}, \quad (5)$$

$$i_{ca} = G_{ca} v_{ca} + \Gamma_{ca} \check{v}_{ca} + C_{ca} v'_{ca}. \quad (6)$$

The measured currents satisfy

$$i_a = i_{ab} - i_{ca}, \quad i_b = i_{bc} - i_{ab}, \quad i_c = i_{ca} - i_{bc}. \quad (7)$$

The full $G\Gamma C$ form is the model used by the sampled-data implementation when the local trajectory has enough rank. To show the geometric core without hiding it inside numerical linear algebra, the analytical derivation is written here for the two-element $G\Gamma$ delta reference. The independent measured variables can be chosen as v_{ab} , v_{bc} , i_a , and i_b . The six-dimensional spacor is

$$\mathbf{y} = v_{ab} \mathbf{e}_1 + v_{bc} \mathbf{e}_2 + \check{v}_{ab} \mathbf{e}_3 + \check{v}_{bc} \mathbf{e}_4 + i_a \mathbf{e}_5 + i_b \mathbf{e}_6. \quad (8)$$

Using $v_{ca} = -(v_{ab} + v_{bc})$, KCL gives

$$i_a = (G_{ab} + G_{ca}) v_{ab} + G_{ca} v_{bc} + (\Gamma_{ab} + \Gamma_{ca}) \check{v}_{ab} + \Gamma_{ca} \check{v}_{bc}, \quad (9)$$

$$i_b = -G_{ab} v_{ab} + G_{bc} v_{bc} - \Gamma_{ab} \check{v}_{ab} + \Gamma_{bc} \check{v}_{bc}. \quad (10)$$

Thus \mathbf{y} lies in a four-dimensional subspace of the six-dimensional measurement space. If

$$\mathbf{K} = \mathbf{a} \wedge \mathbf{b} \wedge \mathbf{c} \wedge \mathbf{d} \quad (11)$$

is the model hypervolume and \mathbf{K}_{osc} is the osculating hypervolume computed from trajectory derivatives through the wedge product, then the identified parameters follow by comparing the scalar coefficients of corresponding blades. Specifically, if $\mathbf{K}_{osc} = \sum_I s_I \mathbf{e}_I$, then s_{ijkl} denotes the scalar coefficient multiplying $\mathbf{e}_i \wedge \mathbf{e}_j \wedge \mathbf{e}_k \wedge \mathbf{e}_l$. The quotients used for the delta parallel $G\Gamma$ model are

$$G_{ab} = \frac{s_{2346}}{s_{1234}}, \quad G_{bc} = \frac{s_{1346}}{s_{1234}}, \quad G_{ca} = \frac{s_{1345}}{s_{1234}}, \quad (12)$$

$$\Gamma_{ab} = \frac{s_{1246}}{s_{1234}}, \quad \Gamma_{bc} = \frac{s_{1236}}{s_{1234}}, \quad \Gamma_{ca} = \frac{s_{1235}}{s_{1234}}.$$

The expanded symbolic forms of the s_I coefficients are provided in the online derivation package at <https://electrica.ual.es/spacor>. The quotients in (12) are exact: each branch parameter equals a fixed ratio of blade coefficients of the osculating hypervolume, so the windowed least squares used later does not discover an arbitrary equivalent—it evaluates, over a finite record, the very linear identities that the geometric construction makes exact. The matrix form is therefore a numerical evaluation of (12), not a generic regression onto KCL regressors.

3) *Three-Wire Wye Series Model*: The directly resolvable wye family in a three-wire load is the series form. Here the measured line currents are the branch currents, with $i_c = -(i_a + i_b)$, while the unknown neutral voltage is eliminated by writing KVL in terms of line-to-line voltages. For a wye series equivalent without measured neutral, the branch equations are

$$v_{xn} = R_x i_x + L_x i'_x + S_x \check{i}_x, \quad x \in \{a, b, c\}. \quad (13)$$

The measurable line voltages are

$$v_{ab} = v_{an} - v_{bn}, \quad v_{bc} = v_{bn} - v_{cn}, \quad v_{ca} = v_{cn} - v_{an}. \quad (14)$$

For the two-element RL series wye model, KVL gives the explicit measured relations

$$v_{ab} = R_a i_a + L_a i'_a - R_b i_b - L_b i'_b, \quad (15)$$

$$v_{bc} = R_b i_b + L_b i'_b + R_c (i_a + i_b) + L_c (i'_a + i'_b). \quad (16)$$

The corresponding geometric construction uses the spacor

$$\mathbf{z} = i_a \mathbf{e}_1 + i_b \mathbf{e}_2 + i'_a \mathbf{e}_3 + i'_b \mathbf{e}_4 + v_{ab} \mathbf{e}_5 + v_{bc} \mathbf{e}_6. \quad (17)$$

Comparing the model hypervolume with the osculating hypervolume gives the same type of s_I -coefficient quotients:

$$\begin{aligned} R_a &= \frac{s_{2345}}{s_{1234}}, & R_b &= \frac{s_{1345}}{s_{1234}}, & R_c &= \frac{s_{2346}}{s_{1234}}, \\ L_a &= -\frac{s_{1245}}{s_{1234}}, & L_b &= \frac{s_{1235}}{s_{1234}}, & L_c &= \frac{s_{1246}}{s_{1234}}. \end{aligned} \quad (18)$$

As for the delta case, the expanded s_I expressions are provided in the online derivation package and remain mechanically auditable. The six branch parameters are recovered from the geometry of the measured $(i_a, i_b, i'_a, i'_b, v_{ab}, v_{bc})$ trajectory, not from a phasor decomposition: (18) is the same blade-coefficient identity for the wye-series family, and the windowed estimator of Section III-A simply evaluates it over a finite window.

4) *Structural Singularities and Virtual-Neutral Model:* The two direct three-wire families above are not arbitrary choices. They are the nonsingular combinations imposed by terminal observability. A parallel wye equivalent would require the absolute phase-to-neutral voltages v_{an} , v_{bn} , and v_{cn} , but three-wire measurements determine only their differences. Adding an arbitrary common-mode function $u(t)$ to all three phase potentials leaves v_{ab} , v_{bc} , and v_{ca} unchanged while changing the branch voltages seen by a parallel wye model. Thus the parameters are not unique without an additional neutral constraint. Conversely, a series delta equivalent would require the internal branch currents i_{ab} , i_{bc} , and i_{ca} . Terminal currents give only their differences; the transformation $(i_{ab}, i_{bc}, i_{ca}) \mapsto (i_{ab} + h, i_{bc} + h, i_{ca} + h)$ leaves i_a , i_b , and i_c unchanged for any circulating component $h(t)$. Since a series branch law depends on the branch current itself, the associated parameters are structurally indeterminate. These are observability singularities of the three-wire measurement problem, not numerical failures.

A useful additional representation is obtained by introducing a virtual neutral. This construction, related to the classical artificial-neutral and $n - 1$ wattmeter viewpoints [12]–[14], does not create a measured physical conductor. It selects a reference node that allows a wye series equivalent to account for terminal behavior when the load is better interpreted as a sum of line-to-line branches. The virtual-neutral example in Section IV-A shows that the identified wye parameters recover the original line-to-line values through branch sums, which is precisely the interpretation expected from the structural singularity of the direct series-delta family.

The singularities resolved here concern parameter observability: within a chosen admissible family, the branch parameters either are or are not recoverable from terminal data. They do not concern the uniqueness of the internal energy localization across admissible families. Two families that are both nonsingular here—for instance the delta parallel and the wye series—can reproduce identical terminal data while localizing stored and dissipated energy differently—a modeling question beyond the terminal identifiability addressed here.

Table I summarizes which branch form each connection makes directly identifiable from its measured terminal variables, and which combinations are structurally singular rather than merely ill-conditioned.

III. FROM GEOMETRIC THEORY TO WINDOWED MATRIX IMPLEMENTATION

A. Geometric and Matrix Identification

The analytical geometric method published for the single-phase case constructs a time-dependent vector whose coordinates are measured waveforms and their derivatives or integrals. Kirchhoff laws confine this trajectory to a lower-dimensional geometric object. Equivalent parameters are obtained by comparing the model subspace with the osculating subspace of the measured trajectory.

In exact symbolic form, the geometric construction yields the closed quotients (12) and (18), in which each branch parameter is a fixed ratio of blade coefficients of the osculating hypervolume. In sampled data, those same blade identities are evaluated over a short window on the order of a single fundamental period—here 0.5–2 cycle windows, about 10–40 ms at 50 Hz—which absorbs noise and lets the construction track slowly varying parameters. The least-squares problem solved per window is not a generic regression; it is the finite-window form of that identity. For a window w , the model is written as

$$\mathbf{y}_w = \Phi_w \theta + \epsilon_w, \quad (19)$$

where $\mathbf{y}_w \in \mathbb{R}^{m_w}$ is the measured output vector, $\Phi_w \in \mathbb{R}^{m_w \times n_\theta}$ is built from the voltage/current coordinates, derivatives, and integrals dictated by KCL or KVL, and $\theta \in \mathbb{R}^{n_\theta}$ collects the unknown branch parameters. The integer n_θ is therefore the number of estimator coordinates required by the selected equivalent; for example, $n_\theta = 6$ for a three-wire delta parallel GT model and $n_\theta = 9$ for a full delta parallel RLC model written in G, T, C coordinates.

Before solving the least-squares problem, the matrix is scaled to remove the arbitrary numerical effect of units. A full-parameter estimate is meaningful only if the scaled local trajectory contains enough information:

$$\text{rank}_\tau(\tilde{\Phi}_w) = n_\theta, \quad \kappa_2(\tilde{\Phi}_w) = \frac{\sigma_{\max}(\tilde{\Phi}_w)}{\sigma_{\min}(\tilde{\Phi}_w)} \leq \kappa_{\max}. \quad (20)$$

Here rank_τ is the numerical rank computed with a tolerance τ , σ_{\max} and σ_{\min} are the extreme singular values of the scaled regressor matrix, and κ_{\max} is a user-defined acceptance threshold. In the MATLAB simulations below, $\kappa_{\max} = 10^6$ is used as a conservative gate. Thus the geometric quotients and the windowed least squares are two evaluations of the same linear identities implied by Kirchhoff's laws and the chosen topology—symbolic on an exact trajectory, numerical on a finite noisy record. The estimator does not select an equivalent; it evaluates the equivalent that the geometry has already fixed.

B. Identifiability and Information Content

The method is not a frequency-domain identification method. Harmonics are not the foundation of the theory. The relevant question is whether the time-domain trajectory spans the geometric dimension required by the chosen equivalent.

Table I
TOPOLOGY-DEPENDENT IDENTIFIABILITY FROM TERMINAL DATA

Connection / wires	Meas. vars	Branch form	Status	Reason
Wye, 4-wire	v_{xn}, i_x	<i>RLS</i> series	I	Phase-to-neutral voltages measured; each phase reduces to single-phase [9].
Delta, 3-wire	v_{xy}, i_x	<i>GTC</i> parallel	I	Branch voltages are the measured line voltages; branch currents from KCL of line currents.
Delta, 3-wire	v_{xy}, i_x	<i>RLS</i> series	S	Needs internal branch currents; a circulating $h(t)$ leaves i_x unchanged.
Wye, 3-wire	v_{xy}, i_x	<i>RLS</i> series	I	Line currents are branch currents; neutral eliminated by KVL in v_{xy} .
Wye, 3-wire	v_{xy}, i_x	<i>GTC</i> parallel	S	Needs absolute v_{xn} ; a common-mode $u(t)$ leaves v_{xy} unchanged.
Virtual neutral	$v_{xn'}, i_x$	<i>RLS</i> series	C	Reference node $\sum v_{xn'} = 0$ is a coordinate device, not a measured conductor; recovers branch sums.

I: identifiable. S: structurally singular (observability singularity, not numerical failure). C: coordinate construction. $\Gamma = 1/L$, $S = 1/C$.

For example, in a single-phase parallel *RLC* model the regressors are v , \dot{v} , and v' . A pure sinusoid satisfies $v' = -\omega^2 \dot{v}$, so the regressors cannot span a three-dimensional space. The same principle explains the three-wire case: pure fundamental data may be sufficient for a resistive model but insufficient for higher-order unbalanced *RL* or *RLC* equivalents. Harmonics, switching, transients, ramps, or modulation can all create the required time-domain rank.

This rank criterion is central to the implementation. Measurement noise is not allowed to "repair" a structurally non-identifiable trajectory; such windows are reported as low-information rather than used as high-confidence evidence.

C. Energy-Admissibility Criterion

Rank and conditioning answer an information question: Can the terminal trajectory support the number of unknowns of the selected equivalent circuit? They do not, by themselves, prove that the recovered parameters define a physically admissible energy model. For this reason each accepted window is also tested by a terminal energy-balance check (for the assumed topology).

Let $p_{\text{PCC}}(t)$ denote the instantaneous terminal power computed from the measured voltage-current coordinates at the PCC. Once a candidate delta or wye equivalent has been identified, the same window gives the irreversible Joule term and the stored electromagnetic energy,

$$p_d(t) = \sum_{r \in \mathcal{R}} R_r i_r^2(t) = \sum_{g \in \mathcal{G}} G_g v_g^2(t), \quad (21)$$

$$W(t) = \frac{1}{2} \sum_{\ell \in \mathcal{L}} L_\ell i_\ell^2(t) + \frac{1}{2} \sum_{c \in \mathcal{C}} C_c v_c^2(t). \quad (22)$$

The energy residual is then

$$\rho_E = \frac{\|p_{\text{PCC}}(t) - p_d(t) - W'(t)\|_2}{\|p_{\text{PCC}}(t)\|_2 + \varepsilon_E}. \quad (23)$$

Here ε_E only prevents division by zero in very low-power windows. Equation (23) is not a new power definition. It is a conservation check: after the equivalent is identified, the measured terminal power must be explainable as dissipated power plus the time derivative of energy stored in the identified L and C elements of the assumed equivalent.

This criterion is important for two reasons. First, it prevents a numerically well-conditioned least-squares fit from being interpreted as a physical equivalent when the recovered elements do not close the energy balance. Second, it separates random measurement noise from coherent measurement-chain biases.

Additive noise broadens ρ_E and the parameter distributions, whereas a current-sensor delay produces a systematic phase error that may pass some rank tests but fails the energy interpretation. Thus the method reports an equivalent as high-confidence only when it is identifiable, passive, Kirchhoff-consistent, and energy-admissible.

D. Sampled-Data Numerical Implementation

The published single-phase theory established the geometric construction and its continuous-time energy-equivalent interpretation [9]. The later experimental validation showed that the single-phase idea can be operated with laboratory measurements [10]. The implementation used here adds a different layer: it turns the exact geometric construction into a finite-window, matrix-based, three-phase estimator with explicit signal-processing and diagnostic steps. This layer is essential for three-wire systems because the missing neutral, the KCL/KVL constraints, and the coexistence of several energy-equivalent families make pointwise symbolic formulae unsuitable for noisy sampled records.

The sampled-data implementation follows these steps:

- 1) form overlapping local windows from the terminal voltage and current records;
- 2) build the matrix pair (Φ, \mathbf{y}) required by the physical equivalent under test;
- 3) compute derivative or primitive coordinates with a configured window-local signal model;
- 4) scale the columns of Φ and the output rows so that conditioning is not dominated by units;
- 5) solve the resulting least-squares problem and convert the estimator coordinates back to physical R , L , and C values;
- 6) compute rank, condition number, coverage, passivity, KCL/KVL residuals, terminal-power residual, and the energy-admissibility residual ρ_E .

This is not merely a different coding style for the analytical formulae. The windowed estimator changes how the method is used. Instead of differentiating a single sample and trusting the resulting quotient, each estimate is supported by all samples in the window and by independent consistency tests. In addition, the same signal record can be tested against delta parallel RLC and wye series RLC families without changing the physical measurements; only the KCL/KVL matrix changes. If the local trajectory cannot support all parameters of a higher-order equivalent, the corresponding rank and conditioning diagnostics make this visible before the parameters are interpreted.

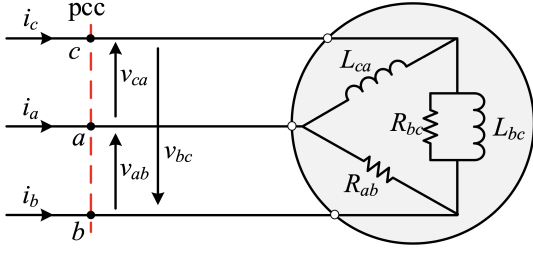


Figure 5. Three-wire unbalanced delta load with nonsinusoidal excitation.

The derivative layer is also new with respect to the theoretical formulation. The implementation avoids high-order pointwise numerical derivatives. The three-wire simulations reported here require primitives or first derivatives only. Derivative coordinates are obtained over the same observation window by a configurable signal estimator: linear-phase FIR differentiators, local polynomial filters, Tikhonov-smoothed finite differences, or harmonic projection followed by analytical differentiation [15], [16]. The harmonic projection is the default for the multisine simulations because it separates the physical low-order spectral content used for excitation from broadband measurement noise. The matrix/windowed procedure is summarized in Appendix A.

For a fixed topology, the computational cost of one window is dominated by forming Φ and solving a small least-squares problem. If the window has N samples and the model has n_θ unknowns, the cost is $O(Nn_\theta^2 + n_\theta^3)$, with $n_\theta \leq 9$ for the three-wire families used in this paper. Thus the method does not rely on a nonlinear search over a large parameter space. Its practical limitation is not the algebraic cost but the availability of informative windows and an appropriate physical equivalent set for the measured feeder.

IV. VALIDATION STRATEGY AND SIMULATION STUDIES

A. Canonical Analytical Identification Cases

The following analytical examples serve as controlled reference cases. Their role is to demonstrate the load-equivalent topologies and the symbolic identification path, while the MATLAB simulations in the next section test numerical robustness under more realistic measurement conditions.

1) *Three-Wire Delta Parallel Case*: The delta example of Fig. 5 is the first core three-wire case. The test load has unbalanced linear RL branches: $R_{ab} = 2.0 \Omega$, $R_{bc} = 1.333 \Omega$, $L_{bc} = 2 \text{ mH}$, and $L_{ca} = 3 \text{ mH}$. Equivalently, $G_{ab} = 0.5 \text{ S}$, $G_{bc} = 0.750 \text{ S}$, $\Gamma_{bc} = 500 \text{ H}^{-1}$, and $\Gamma_{ca} = 333.3 \text{ H}^{-1}$.

The line-to-line voltages used in this controlled test are

$$v_{ab} = 120 \cos 100\pi t + 90 \cos 400\pi t + 108 \cos 1600\pi t, \quad (24)$$

$$v_{bc} = 132 \cos(100\pi t - \pi/3) + 100 \cos(400\pi t - 2\pi/3) + 120 \cos(1600\pi t - 2\pi/3), \quad (25)$$

$$v_{ca} = -(v_{ab} + v_{bc}). \quad (26)$$

These waveforms provide the geometric rank needed by the GF delta model, so the exact GA quotients and the windowed matrix estimator return the same branch constants in the noise-free case. The waveforms and identified parameters are shown in Figs. 6 and 7.

The terminal waveforms in Fig. 6 are strongly nonsinusoidal, so the local trajectory spans the full rank required by the GF

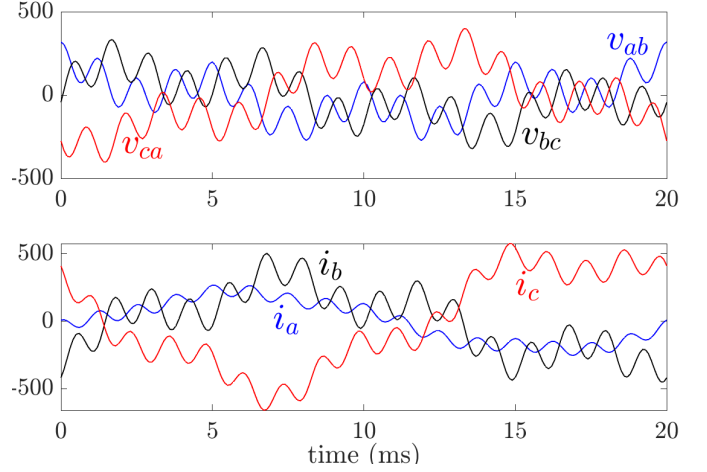


Figure 6. Voltage and current waveforms for the delta case.

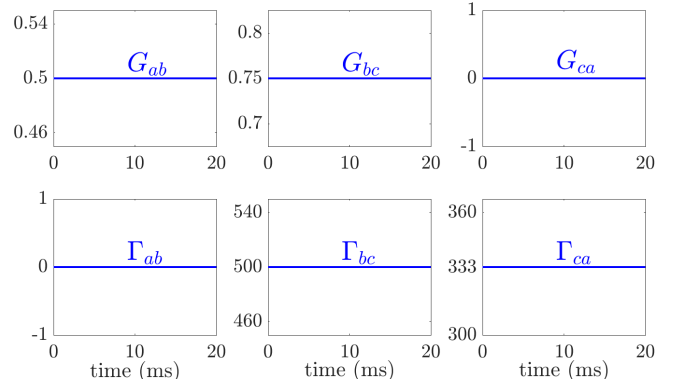


Figure 7. Delta identification result. This case is the clean reference for noise, window, and delay studies.

delta model. The identification is then exact: every window in Fig. 7 returns $G_{ab} = 0.5 \text{ S}$, $G_{bc} = 0.75 \text{ S}$, $\Gamma_{bc} = 500 \text{ H}^{-1}$, and $\Gamma_{ca} = 333.3 \text{ H}^{-1}$ as flat lines with no scatter, and the structural zeros $\Gamma_{ab} = 0$ (purely resistive ab branch) and $G_{ca} = 0$ (purely inductive ca branch) are recovered without spurious leakage. In this noise-free reference the windowed estimator matches the analytical GA quotients to numerical precision.

2) *Three-Wire Wye Series Case*: The second core three-wire case is the series wye load of Fig. 8. The current-source excitation used in this controlled case is

$$i_a = 120 \cos \omega t + 10 \cos 5\omega t, \quad (27)$$

$$i_b = 240 \cos(\omega t - 2\pi/3) + 10 \cos(5\omega t - 10\pi/3), \quad (28)$$

$$i_c = -i_a - i_b. \quad (29)$$

The branch parameters were $R_a = 0.5 \Omega$, $R_b = 0 \Omega$, $R_c = 7 \Omega$, $L_a = 3 \text{ mH}$, $L_b = 7 \text{ mH}$, and $L_c = 0$. This example is kept because it demonstrates that the three-wire wye problem is solvable when formulated as a series branch problem driven by KVL.

3) *Virtual Neutral Case*: The virtual-neutral construction is also preserved, but with a clearer role: it is an identification coordinate system, not a hidden physical neutral. This idea is connected with Blondel's polyphase measurement theorem and

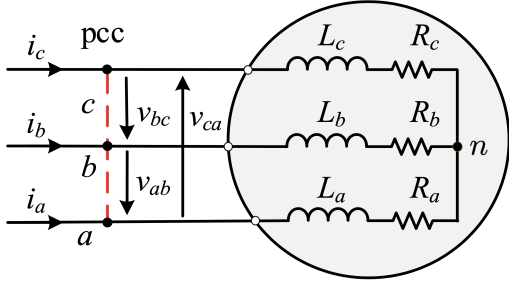


Figure 8. Unbalanced three-wire wye series load.

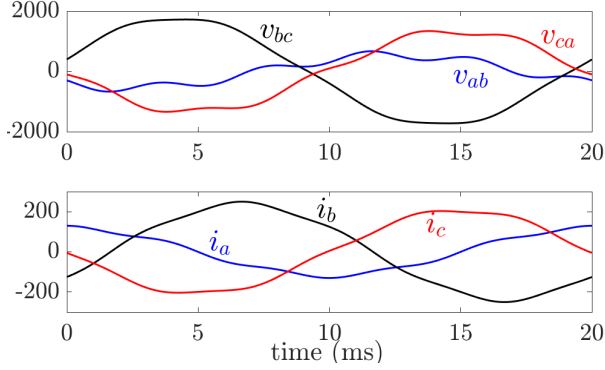


Figure 9. Line-to-line voltages and line currents for the wye series case.

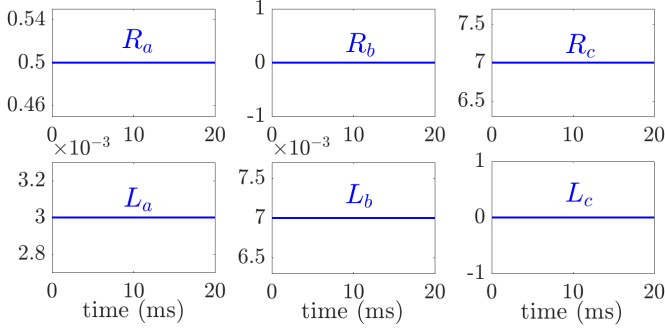


Figure 10. Wye series identification result, reported together with rank and residual diagnostics.

with the Fryze-Buchholz-Depenbrock time-domain framework [12]–[14]. From the line voltages,

$$v_{an'} = \frac{1}{3}(v_{ab} - v_{ca}), v_{bn'} = \frac{1}{3}(v_{bc} - v_{ab}), v_{cn'} = \frac{1}{3}(v_{ca} - v_{bc}), \quad (30)$$

which ensures $v_{an'} + v_{bn'} + v_{cn'} = 0$. This allows the use of phase-wise single-phase identification with $i_{n'} = 0$ when the chosen equivalent is a virtual wye model. The virtual-neutral test uses a strongly unbalanced RL branch with $R_{ab} = 0.306 \Omega$ and $L_{ab} = 0.7755 \text{ mH}$, energized at $\omega = 200\pi \text{ rad/s}$ by

$$\begin{aligned} v_{ab} &= 130\sqrt{2} \cos \omega t, \\ v_{bc} &= 120\sqrt{2} \cos(\omega t - 2\pi/3), \\ v_{ca} &= -(v_{ab} + v_{bc}). \end{aligned}$$

The identified virtual-wye sums recover the physical branch values: $R_a + R_b = 0.306 \Omega$ and $L_a + L_b = 0.7755 \text{ mH}$.

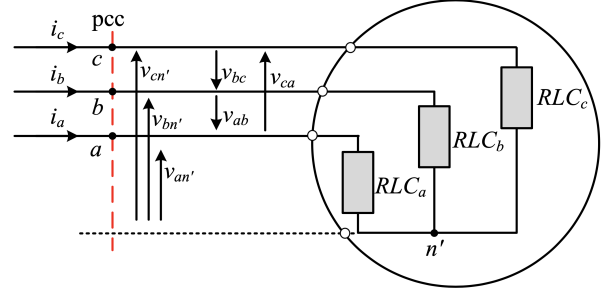


Figure 11. Virtual-neutral wye model for three-wire identification.

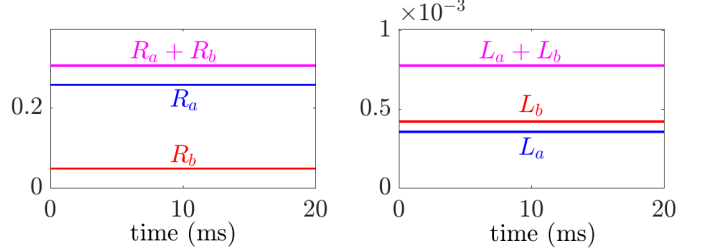


Figure 12. Virtual-neutral identification result. The key reported value is the recovered sum of virtual branch parameters.

B. Realistic MATLAB Simulations

The preceding examples establish the algebraic structure of the proposed three-wire equivalents. They do not, by themselves, answer the practical question raised by sampled measurements: whether the physical equivalent can still be recovered when the observer has only finite windows of noisy terminal waveforms. The MATLAB simulations in this section address that question. Their purpose is not to benchmark a generic system-identification routine or to force an answer for every possible waveform; it is to test whether the method recovers a correct load-equivalent model when the measurement record contains sufficient information, and whether the diagnostic quantities expose cases that are poorly conditioned or biased by the measurement chain. This study is simulation-only by design: it isolates the three-phase identifiability problem under controlled, known-ground-truth conditions. Laboratory validation of the single-phase formulation is reported in [10], and three-phase hardware validation is left to future work, but there is a high degree of confidence since single phase cases were properly validated with strenuous circumstances.

Two sets of simulations are used. The first set is a topology-and-order study, covering balanced and unbalanced delta parallel RLC and wye series RLC loads, including an extreme-unbalance case and a deliberately low-information single-frequency case. The second set is a measurement-chain stress study applied to a fully unbalanced three-wire delta parallel RLC load. This second case is intentionally demanding because all branch resistances, inductances, and capacitances must be recovered from terminal line-to-line voltages and line currents.

All simulated records are generated from a 50 Hz unbalanced multisine source sampled at 20 kHz. The phase voltages include amplitude imbalance and low-order harmonics,

$$v_x(t) = \sum_{h \in \mathcal{H}_x} V_{x,h} \sin(h\omega_0 t + h\phi_x + \alpha_{x,h}), \quad x \in \{a, b, c\}. \quad (31)$$

Table II
BASELINE SAMPLED-DATA CHECKS FOR THE THREE-WIRE
IMPLEMENTATION.

Case	Coverage	Median cond.	Power residual
Delta clean	1.00	21.83	5.30×10^{-16}
Delta 60 dB	1.00	21.83	1.51×10^{-3}
Wye clean	1.00	3.52	1.61×10^{-14}
Wye 60 dB	1.00	3.52	2.95×10^{-3}

so the estimator is not using a phasor model extracted from ideal sinusoids. For every run, the input data are only the terminal waveforms available at the three-wire point of connection. Each sliding window spans 0.75 of a fundamental cycle (15 ms, i.e. 300 samples at 20 kHz) and advances in steps of 0.10 cycle (2 ms); the windows are processed independently. For each window, the implementation computes the rank and condition number of the regression matrix, KCL/KVL consistency, terminal power residual, energy residual, passivity, and physical parameter estimates. The internal delta parallel coordinates G, I, C are converted back to the reported physical parameters $R = 1/G$, $L = 1/I$, and C .

Table II gives a compact baseline check. The clean cases close the terminal power balance at machine precision, while the 60 dB cases increase the residual to the level expected from the injected measurement noise. This table is deliberately simple: it verifies that the sampled-data implementation preserves the exact geometric construction before the more demanding stress cases are considered.

Fig. 13 then shows the main reporting style for one representative stress case. The upper panel displays five cycles of the measured terminal voltages and currents. The lower panels show the recovered branch R , L , and C values in engineering units for successive windows; dashed lines are the known parameters used to synthesize the load. This figure is important because it avoids hiding the method behind regression coordinates: the reader sees the measured waveforms and the physical load-equivalent parameters that are recovered from them.

The measurement-chain stress study applies the perturbations that are most likely to degrade this type of time-domain estimator: white measurement noise at 60 dB and 40 dB SNR, 12-bit quantization, voltage/current gain mismatch, a 50 μ s coherent current-sensor delay, and the combined delay-plus-noise case. Practical window lengths from 0.5 to 2 cycles are shown in Fig. 14; deliberately fragile 0.25-cycle windows are retained in the reproducibility data set but excluded from the main figure. The boxes summarize the distribution of relative errors over branch R , L , and C estimates. Clean data, 60 dB noise, 40 dB noise, 12-bit quantization, and gain mismatch remain within the 5% engineering band in all practical-window settings. Current-sensor delay is different: it produces a coherent phase bias rather than random scatter, and the resulting parameter errors are therefore correctly visible as a synchronization problem rather than as an uncertainty that can be averaged away.

The same observations are summarized in Table III. It separates three situations that must not be conflated. First, low-rank waveforms, such as a pure fundamental excitation for a high-order RLC equivalent, are not informative enough to identify all stored-energy coordinates. Second, additive

noise and quantization mainly broaden the error distribution; their effect is reduced by informative windows of practical length. Third, coherent timing error is a bias in the measured relationship between voltage and current; it must be calibrated or diagnosed, not treated as zero-mean noise.

For the degradation study in Fig. 14, a configuration is considered high-confidence when

$$\begin{aligned} \text{coverage} &\geq 80\%, & \text{max relative error} &\leq 5\%, \\ \rho_E &\leq 5\%, & \kappa &\leq 10^6. \end{aligned} \quad (32)$$

Fifteen of the 21 practical-window configurations in the degradation study satisfy this gate. The six configurations that do not satisfy it are precisely the current-delay and delay-plus-noise cases. This is the desired behavior for a field method: the estimator should recover physical parameters under ordinary measurement noise and quantization, but it should not disguise a coherent synchronization error as a reliable load equivalent.

The additional derivations, expanded s_I coefficients, nine-case topology/operating-condition summaries, degradation heat maps, window diagnostics, extra waveform-parameter examples, and MATLAB reproduction scripts are maintained as online material at <https://electrica.ual.es/spacor>. The printed paper keeps only the figures needed to support the principal claims.

V. DISCUSSION

The method identifies an equivalent only when the measured trajectory contains the information required by the candidate model. This is essential for field use. An algorithm that always returns parameters can be numerically convenient but physically misleading. The proposed diagnostics make the result auditable: one can see whether the model is passive, whether Kirchhoff constraints are satisfied, whether the energy-admissibility residual is small, and whether the local geometry is sufficiently rich. This is more than an error metric: it is the physical test that connects parameter identification with the energy equivalent for the assumed topology reported in the same observation window.

When several admissible topologies pass the rank, conditioning, and energy-admissibility tests, they are terminally indistinguishable from the given window: each closes the same terminal energy balance while assigning the stored and dissipated energy to different branches. One then reports the admissible alternatives or resorts to a prior topology or additional excitation, since no selection rule exists at the level of terminal data alone; characterizing that non-uniqueness is a separate, energy-level question.

The present manuscript also clarifies the relation between exact geometric formulae and practical sampled-data implementation. The symbolic quotients establish the analytical structure of the identifiable models, while the windowed matrix form is the implementation used to address noise, derivatives, conditioning, and computational feasibility.

Compared with event-driven aggregate load identification and other time-varying parameter approaches [3], [5], the proposed estimator is narrower but more physically structured: it identifies the parameters of a selected load equivalent directly from local terminal waveforms. It should therefore be judged by whether the selected topology is identifiable, passive, and energetically consistent in the observation window, not by whether it can emulate arbitrary black-box dynamics.

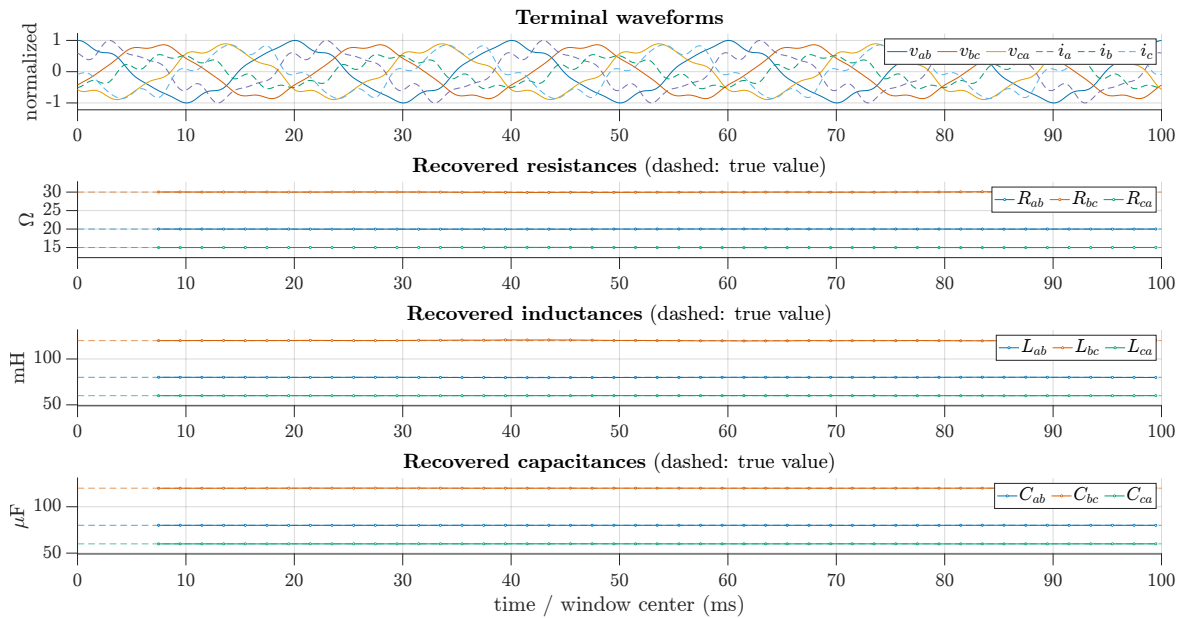


Figure 13. Representative three-wire delta parallel RLC identification under 70 dB measurement noise. The upper panel shows the measured terminal waveforms over five cycles. The lower panels show recovered resistances, inductances, and capacitances in physical units. Dashed lines indicate the known values used to synthesize the load.

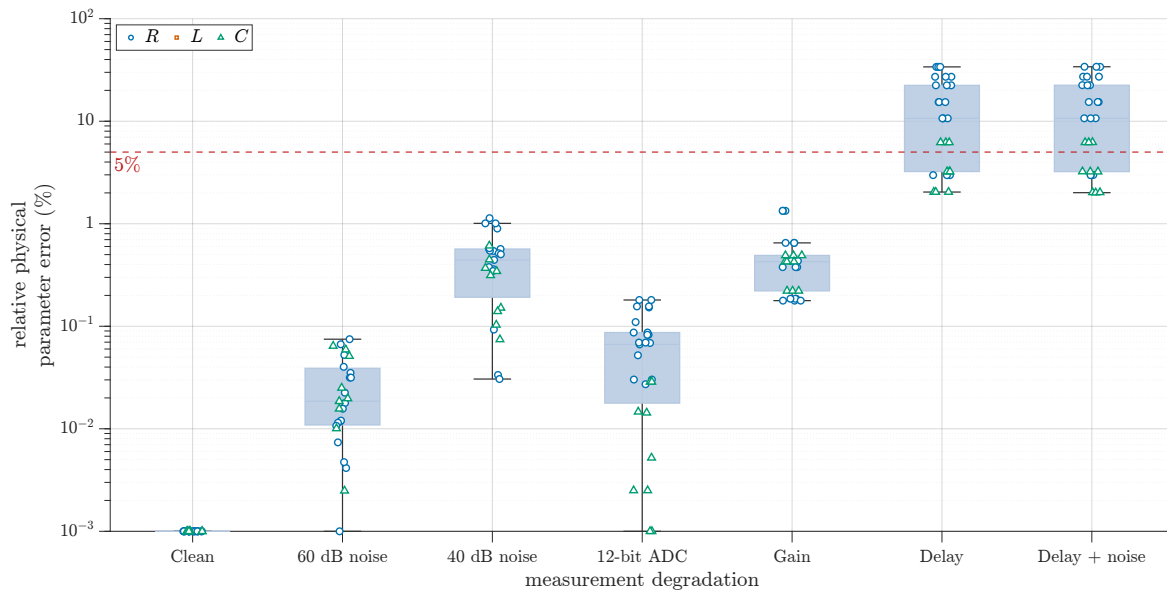


Figure 14. Measurement-chain stress test for a three-wire delta parallel RLC load. Boxes summarize the distribution of relative physical-parameter error across branch R , L , and C estimates and practical window lengths from 0.5 to 2 cycles; markers show the individual element classes. The dashed line marks 5%. The deliberately fragile 0.25-cycle windows are retained in the reproducibility data set but excluded from this main-paper view.

Table III
REPRESENTATIVE BEHAVIOR OF THE REALISTIC THREE-WIRE MATLAB STUDY.

Scenario	Main observation	Information content
Pure fundamental	The trajectory is rank deficient for higher-order three-wire RLC models. Noise may create numerical rank but not physical information.	Insufficient
Weak harmonics, clean	Parameters are recovered when the window is at least 0.5 cycles; shorter windows are fragile.	Sufficient
Weak harmonics, 60 dB	Residuals remain compatible with injected noise for 0.5–2 cycle windows.	Sufficient
Weak harmonics, 40 dB	Longer windows, typically 1–2 cycles, are required for stable estimates.	Conditional
Rich harmonics	Conditioning improves markedly; median condition is about 22 for delta parallel and 3.5 for wye series in the tested cases.	Sufficient
50 μ s current delay	The error is coherent rather than random; delta parallel RLC reaches about 37% maximum parameter error in the stress test, despite otherwise acceptable rank and coverage.	Biased

VI. CONCLUSIONS

This paper identifies three-phase load equivalents from terminal measurements in the time domain, with particular attention to the three-wire case. The implementation adds the practical layer required for sampled data: finite windows, normalization, explicit identifiability tests, measurement-degradation studies, and energy-admissibility validation. The practical value is that the result is an equivalent circuit with the same energetic behavior as the measured load: energy is consumed and stored or restored in the same fashion as in the physical circuit. The identified equivalents therefore provide the physical state required for element-level energy accounting within the recovered load model and for monitoring, protection, or compensation applications.

Several applications follow from this capability. Because the equivalent is recovered from local windows of terminal data and needs no neutral connection, it suits three-wire distribution feeders, motor and delta-connected loads, and converter interfaces where only line quantities are accessible. Tracking the recovered branch R , L , and C across windows turns the method into a condition-monitoring tool, with the energy-admissibility and conditioning diagnostics separating genuine parameter drift from measurement artefacts such as the coherent sensor delay reported above. The same physically meaningful equivalent supports impedance-based and adaptive converter control, relay setting and anomaly detection in protection, and the sizing of compensation hardware. In all of these the confidence gate is decisive for field use: the estimator either returns an auditable equivalent or declares the window uninformative, rather than a value that cannot be trusted.

APPENDIX A WINDOWED MATRIX AND HARMONIC-PROJECTION IMPLEMENTATION

Let $z[k]$, $k = 0, \dots, N - 1$, denote any measured terminal waveform in one local window. The implementation first builds the signal coordinates required by the selected physical equivalent. For example, a delta parallel RLC branch uses v_{xy} , \dot{v}_{xy} , and v'_{xy} , whereas a wye series RLC branch uses current coordinates and their corresponding derivatives or primitives. Stacking all samples in the window gives

$$\mathbf{y}_w = \Phi_w \theta + \epsilon_w, \quad (33)$$

where w denotes the window index. Before solving, the columns and output are scaled as

$$\tilde{\Phi}_w = \mathbf{W}_y \Phi_w \mathbf{W}_\theta^{-1}, \quad \tilde{\mathbf{y}}_w = \mathbf{W}_y \mathbf{y}_w, \quad (34)$$

with diagonal scale matrices computed from column and output norms. The least-squares estimate is obtained from the scaled system and then mapped back to physical units:

$$\hat{\theta}_w = \mathbf{W}_\theta^{-1} \tilde{\Phi}_w^\dagger \tilde{\mathbf{y}}_w. \quad (35)$$

The reported condition number is the condition of the scaled problem, so it measures information content rather than the arbitrary choice of volts, amperes, henries, or farads.

The harmonic-projection derivative used in the multisine simulations is a window-local model, not a frequency-domain power decomposition. A measured signal is approximated by

$$z(t) \approx c_0 + \sum_{h \in \mathcal{H}_w} [a_h \cos(h\omega_0 t) + b_h \sin(h\omega_0 t)], \quad (36)$$

where \mathcal{H}_w is either prescribed or selected from candidate harmonics using relative amplitude, energy fraction, sample budget, and basis conditioning. Differentiation is then analytical:

$$\frac{d^q z}{dt^q} \approx \sum_{h \in \mathcal{H}_w} (h\omega_0)^q \left[a_h \cos\left(h\omega_0 t + \frac{q\pi}{2}\right) + b_h \sin\left(h\omega_0 t + \frac{q\pi}{2}\right) \right]. \quad (37)$$

For primitive coordinates, the same fitted harmonics are integrated analytically after removing the local mean; when a direct integral form is available, it is preferred over a differentiated form because it is less sensitive to quantization.

Each window produces not only $\hat{\theta}_w$, but also a health record:

$$\mathcal{D}_w = \{\text{rank}(\tilde{\Phi}_w), \kappa(\tilde{\Phi}_w), \rho_{\text{KCL/KVL}}, \rho_p, \rho_E, \Pi\}, \quad (38)$$

where $\rho_{\text{KCL/KVL}}$ is the equation residual, ρ_p is the terminal-power residual, ρ_E is the energy-admissibility residual defined in (23), and Π records passivity of the recovered elements. This diagnostic record is what allows the method to distinguish an informative noisy window from a low-rank or synchronization-biased one.

REFERENCES

- [1] A. Arif, Z. Wang, J. Wang, B. Mather, H. Bashualdo, and D. Zhao, "Load modeling—a review," *IEEE Transactions on Smart Grid*, vol. 9, no. 6, pp. 5986–5999, 2017.
- [2] J. V. Milanovic, K. Yamashita, S. Martinez Villanueva, S. Z. Djokic, and L. M. Korunovic, "International industry practice on power system load modeling," *IEEE Transactions on Power Systems*, vol. 28, no. 3, pp. 3038–3046, 2012.
- [3] H. Renmu, M. Jin, and D. J. Hill, "Composite load modeling via measurement approach," *IEEE Transactions on Power Systems*, vol. 21, no. 2, pp. 663–672, 2006.
- [4] V. Knyazkin, C. A. Canizares, and L. Soder, "On the parameter estimation and modeling of aggregate power system loads," *IEEE Transactions on Power Systems*, vol. 19, no. 2, pp. 1023–1031, 2004.
- [5] C. Wang, Z. Wang, J. Wang, and D. Zhao, "Robust time-varying parameter identification for composite load modeling," *IEEE Transactions on Smart Grid*, vol. 10, no. 1, pp. 967–979, 2017.
- [6] D. Hestenes and G. Sobczyk, *Clifford Algebra to Geometric Calculus: A Unified Language for Mathematics and Physics*. Springer Science & Business Media, 2012, vol. 5.
- [7] A. Macdonald, *Linear and Geometric Algebra*. Alan Macdonald, 2010.
- [8] T. Hong and F. De Leon, "Lissajous curve methods for the identification of nonlinear circuits: Calculation of a physical consistent reactive power," *IEEE Transactions on Circuits and Systems I: Regular Papers*, vol. 62, no. 12, pp. 2874–2885, 2015.
- [9] F. G. Montoya, F. de Leon, F. M. Arrabal-Campos, and A. Alcayde, "Determination of instantaneous powers from a novel time-domain parameter identification method of non-linear single-phase circuits," *IEEE Transactions on Power Delivery*, vol. 37, no. 5, pp. 3608–3619, 2022.
- [10] F. M. Arrabal-Campos, F. G. Montoya, J. Ventura, S. Sánchez-Acevedo, R. E. Torres-Olguin, and F. De Leon, "Experimental verification of a time-domain load identification method for single-phase circuits," *IEEE Transactions on Power Delivery*, 2025.
- [11] F. G. Montoya, F. de Leon, F. M. Arrabal-Campos, and A. Alcayde, "Branch-level energy localization in three-phase loads: Resolving indeterminacy in time-domain," 2026. [Online]. Available: <https://arxiv.org/abs/2606.07076>
- [12] A. Blondel, "Measurement of energy of polyphase currents," in *Proceedings of the International Electrical Congress, Chicago*, 1893, pp. 112–117.
- [13] M. Depenbrock, "Active and nonactive power components of periodic currents in single- and multi-conductor systems with periodic voltages of arbitrary waveform," *ETG Special Report*, vol. 6, pp. 17–59, 1980.
- [14] V. Staudt, "Fryze-buchholz-depenbrock: A time-domain power theory," in *2008 International School on Nonsinusoidal Currents and Compensation*. IEEE, 2008, pp. 1–12.
- [15] S. Paquelet and V. Savaux, "On the symmetry of fir filter with linear phase," *Digital Signal Processing*, vol. 81, pp. 57–60, 2018.
- [16] C.-C. Tseng and S.-L. Lee, "Design of digital differentiators using weighted least squares method," *Signal Processing*, vol. 92, no. 3, pp. 813–824, 2012.